A Dynamically Reconfigurable ECG Analog Front-End with a 2.5× Data-Dependent Power Reduction

Somok Mondal[1], Chung-Lun Hsu[1], Roozbeh Jafari[2], Drew Hall[1]
[1]University of California, San Diego [2]Texas A&M University

***Abstract* —This work addresses a fundamental drawback of conventional bio-signal acquisition interfaces by incorporating a reconfigurable analog front-end (AFE) that can be configured to always operate in an optimal power mode through digital assistance. Implemented in 65 nm CMOS, the AFE has tunable noise performance exhibiting an input-referred noise ranging from 1.90-2.91 μV_{RMS} while consuming 307-769 nW power from a 0.8 V supply. The low activity and quasi-periodicity of bio-signals are exploited using an LMS-based adaptive linear predictive filter for power reduction. An agile, on-the-fly dynamic noise-power reconfiguration strategy is used to achieve data-dependent power savings of 2.5× without compromising the system's anomaly detection capability or ability to extract pristine ECG features.**

I. Introduction

Mobile health sensors, in the form of wearable devices and patches, have tremendous potential for enabling early detection, diagnosis, and real-time monitoring of numerous disorders by continuously and unobtrusively acquiring physiological data in the comfort of one's daily routine. However, this uninterrupted and continuous signal acquisition necessitates low-power circuits to ensure long-lasting, portable operation. For low power bio-signal acquisition systems, a physiological sensing analog front-end (AFE) consisting of a low-noise amplifier and an ADC followed by local real-time bio-feature extraction using analog circuitry [1] or a DSP back-end [2] to remove/reduce the RF transmission requirements is widely accepted as the state-of-the-art. Yet, the AFE in such a conventional system suffers from several drawbacks: 1) The AFE parameters (e.g., amplifier noise, gain, BW, etc.) are fixed at design time and 2) The AFE is designed for worst-case scenarios (e.g., signals corrupted with motion artifacts and/or strong power-line interference). Both of which result in a system that is overdesigned and consumes higher power than needed under typical scenarios. To address the fixed parameter issue, recent works [2-4] have the ability to tune the gain and/or bandwidth of the AFE, but lack the ability to dynamically trade power for the desired performance. As is demonstrated in this work, by utilizing feedback from the DSP, a reduction in the AFE power is possible by reconfiguring the AFE on the fly to always operate in lowest possible power mode.

Most bio-signals are low activity and quasi-periodic, which provides a unique opportunity to enable the use of such a digitally-assisted system. A digitally-controlled dynamic reconfiguration of the AFE is performed to exploit these signal properties for data-dependent power reduction in this work. The concept of leveraging signal properties has been previously used in recent works on SAR ADCs where ~2.5× reduction in the ADC power was achieved by using the previous conversion result as the starting point for the current conversion [5-6]. However, a survey of relevant works indicates that the power of the noise-limited amplifier in most state-of-the-art ECG AFEs is generally 10× times larger than that of the low resolution, low speed SAR ADC [1-2]. For example, the ECG AFE presented in [1] dissipates only 67 nW in the ADC, but 559 nW in the amplifier. It is therefore important to emphasize the amplifier power rather than the ADC power to achieve more substantial power savings.

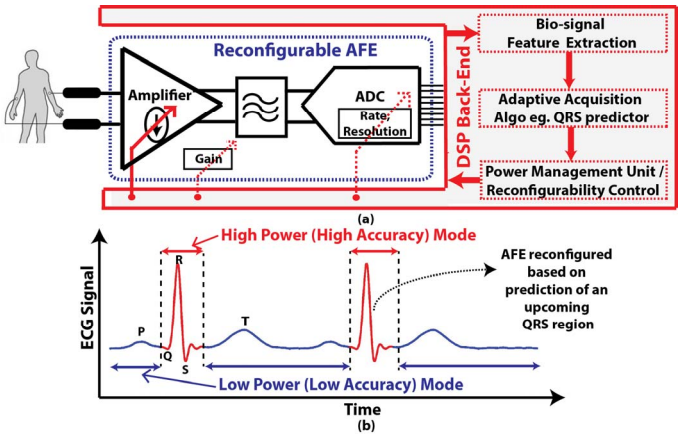

Fig. 1. (a) Proposed digitally-assisted adaptive bio-signal acquisition system architecture. (b) Example of a reconfiguration strategy for an ECG signal.

The work presented in this paper hence demonstrates a data-dependent reduction in an ECG acquisition AFE with the help of a dynamic noise-power trade-off functionality in the power-dominant amplifier. This is guided by an additional component in the DSP back-end – an adaptive predictor based on an least mean squares (LMS)-filter. The rest of this paper is organized as follows: Section II presents the proposed architecture. The AFE circuit and DSP back-end are discussed in Sections III and IV. Measurement results are presented in Section V and a conclusion in Section VI.

II. Adaptive Acquisition System

The proposed digitally-assisted system is shown in Fig. 1(a). The AFE has multiple digitally controllable knobs, most notably, the amplifier noise, which can be dynamically reconfigured to adaptively trade the signal fidelity with power consumption. Other tunable parameters include the amplifier gain and the ADC sampling rate/resolution to aid in efficient signal acquisition. A dynamic time warping (DTW) technique is used to extract bio-signal features in the back-end DSP. As

This work was supported in part by the UCSD Center for Wireless Communication. Chip fabrication support was partially covered by SRC.

978-1-5090-5191-5/17/$31.00@2017 IEEE

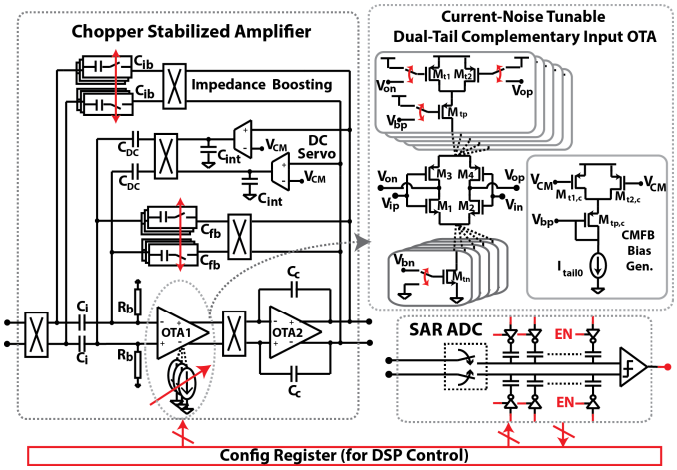

Fig. 2. Schematic of the reconfigurable analog front-end.

shown in Fig. 1(b), an ECG signal is characterized by the P-Q-R-S-T peaks, which are detected in real-time by the DTW. Also evident from Fig. 1(b) is that the QRS complex in an ECG occurs only over a small fraction of the period (less than 15%) and repeats continuously in a well-defined, predictable fashion. As will be shown later, for some applications, it is only critical to acquire the high-activity regions or regions around the peaks of interest with high fidelity for the signal processing thereby creating an opportunity for data-dependent savings like the one illustrated in the example in Fig. 1(b). The dynamic noise-power reconfiguration is directed by an LMS-based adaptive linear predictive filter. With only one prediction per heartbeat needed, this extra component in the system operates at a very slow rate (i.e., for R-peak prediction, with a typical heart-rate of 72 beats/min, the digital filter operates at about 1 Hz) thereby imposing a negligible power overhead and making data-dependent savings using the proposed technique feasible.

III. Reconfigurable AFE: Circuit Description

The reconfigurable analog circuitry implemented for the proposed system is shown in Fig. 2. The low-noise amplifier uses a chopper-stabilized topology to mitigate the otherwise dominant flicker noise [7-8]. To address additional application-specific issues of electrode polarization offset and degraded input impedance due to chopping, a DC servo loop and a positive-feedback impedance boosting loop are employed, respectively. Arrays of switchable feedback capacitors C_{fb} are used to tune the amplifier gain and the impedance boosting capacitors C_{ib} are tuned in tandem with C_{fb} to maintain constant input impedance. The current of the first-stage OTA is tunable over a wide range (100 nA – 675 nA) to offer a fine-grain control over the noise power tradeoff.

The first-stage OTA is implemented using a dual-tail complementary input pair topology (Fig. 2) rather than a conventional single tail version. This allows for a wide current tuning-range as both top and bottom tails can be switched simultaneously without significantly affecting output common-mode voltage and thereby relaxing the common-mode feedback (CMFB) circuit requirements. However, with the agile mode switching required, a simple resistive divider for the CMFB as in [2] is not suitable since the OTA's open loop gain

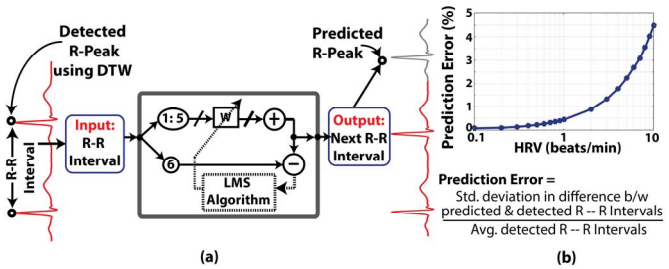

Fig. 3. Adaptive linear predictor (a) functionality and (b) performance.

$g_{\mathrm{m}}(r_{\mathrm{o}}||R_{\mathrm{cmfb}})$ would change with its bias current and cause distortions while switching modes. One approach to overcome this issue is to make R_{cmfb} much larger than the OTA's output impedance, r_{o}. However, this can be challenging in practice. We instead use the CMFB structure shown in Fig. 2 where each PMOS tail cell utilizes transistors $M_{\mathrm{t1,2}}$ as linear resistors in deep triode to set the OTA's output common-mode voltage to V_{CM} while presenting a high impedance capacitive load. The amplifier is designed such that OTA1 with its CMFB consumes 80-540 nW, OTA2 consumes 40 nW, the servo loop consumes 24 nW, and the remaining biasing network and digital circuitry consume 100 nW. In the SAR ADC, resolution reconfiguration (5- to 9-bit) with efficient power-scaling is achieved with the bottom plates of the CDAC driven by tristate inverter buffers such that each resolution decrement is performed by floating the MSB capacitor(s) and starting the conversion from the next largest capacitor. Finally, for adaptive acquisition using the AFE, the mode switching of the amplifier is synchronized with the ADC sampling, such that any perturbations get the maximum settling time. For such low bandwidth and low speed requirements associated with bio-signal acquisition, the amplifier tail current reconfigurations are considerably instantaneous as indicated by simulations during the design phase and confirmed by measurement results presented later.

IV. DSP Back-End

The DSP back-end in the proposed system requires an ECG feature extractor, as in all conventional systems, plus a predictor to control the amplifier reconfiguration. Several algorithms such as the discrete wavelet transform (DWT) [9] or DTW [10] can be used for the real-time detection and classification of ECG features. In this work, the DTW algorithm was chosen and implemented. Using DTW, each data point in a single cycle ECG template along with its distinctive feature gets monotonically mapped to a corresponding point/feature in the acquired ECG, thereby detecting the P-Q-R-S-T peaks [10]. It should be noted that the AFE reconfiguration strategy and LMS filter are independent of the feature extraction algorithm used.

An adaptive linear predictive filter (Fig. 3a) then takes the detected features (e.g., the current and past R-R intervals) and uses an LMS algorithm to predict the upcoming features (e.g., the next R-R interval). A 5$^{\mathrm{th}}$ order filter was found to be sufficiently accurate in predicting features in ECG signals due to the slowly varying nature of the signals. Fig. 3(b) shows this prediction ability and accuracy evaluated using ECG signals with behaviorally added random heart-rate variability (HRV). This adaptive filter is implemented as follows:

$$y[n] = w_1[n]x[n-1] + w_2[n]x[n-2] + \cdots + w_N[n]x[n-N] \quad (1)$$

$$e[n] = y[n] - x[n] \quad (2)$$

$$w_i[n+1] = w_i[n] + x[n-i]e[n]\mu \quad (3)$$

where $w_i[n]$ are the filter coefficients that are adapted to minimize the error $e[n]$ between the predicted R-R intervals $y[n]$ and the ones detected $x[n]$ based on an LMS algorithm with adaptation parameter μ and order N. The performance of such an adaptive filter for the proposed dynamic reconfiguration was previously presented and studied for heart-rate variability detection [11].

The DSP is implemented off-chip on an FPGA for evaluation of other predictors and flexibility. However, the extra component – the LMS filter – if integrated on-chip would contribute to a negligible overhead owing to its operation at ~1 Hz for one prediction per beat as discussed earlier. Furthermore, during regular operation with fairly consistent cardiac activity, the adaptive filter coefficients converge to realize a moving average filter implying that the circuit activity is often quite low. SPECTRE simulations of a synthesized LMS filter in 65 nm CMOS consume less than 10 nW.

V. Measurement Results

Measurements from the chip in 65 nm CMOS with 2 mm^2 area including pads operated from 0.8 V supply are as follows.

A. Reconfigurable AFE

The AFE offers several programmable gain (22-43 dB) modes and the measured bandwidth at 35 dB gain mode is 250 Hz. As shown in Fig. 4, chopping at 4 kHz frequency (more than twice the measured 1/*f* corner of 1.15 kHz) mitigates the otherwise dominant flicker noise. Fine-grain control of the input-referred white noise floor from 125-195 nV/$\sqrt{\text{Hz}}$ is achieved by trading power in 12 uniform steps from 272-734 nW with OTA2 in its lowest power mode (Fig. 4). The measured amplifier input impedance was improved from 6.5 MΩ to 105 MΩ by enabling the impedance boosting loop. A common-mode rejection ratio (CMRR) >82 dB across all modes was measured. The SAR ADC consumes 34.6 nW and 9.1 nW in the 9- and 5-bit modes, respectively. In the 9-bit mode, the ADC has an ENOB of 8.75 bits, a DNL of +0.43/-0.8 LSBs, INL of +0.58/-0.47 LSBs, and an SFDR of 67.1 dB measured at 1 kSps. The linearity performance remains consistent up to10 kSps.

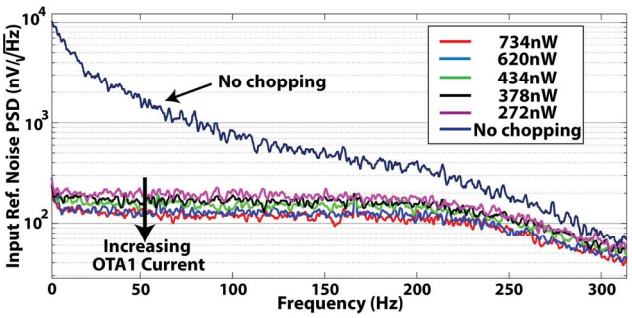

Fig. 4. Amplifier input referred noise PSD in 35 dB gain mode.

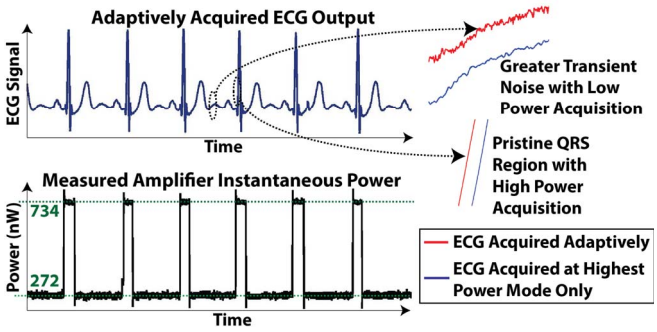

Fig. 5. Measured ECG signal along with measured instantaneous power while performing dynamic reconfiguration to selectively capture the QRS complex with higher accuracy.

B. Adaptive Acquisition

With the QRS-complex of an ECG being its most distinctive feature and its periodicity, width, variability in amplitude, etc. providing crucial diagnostic information, the adaptive acquisition is demonstrated for an application wherein only the Q-R-S detection accuracy is critical. Measured ECG showing the discerning compromise with signal quality in low power mode, and instantaneous power indicating an agile mode switching leading to a 2.5× data-dependent power savings are shown in Fig. 5. Although only high fidelity Q-R-S acquisition is demonstrated here, with the ability to predict each of the P-Q-R-S-T peaks individually, the concept could be extended to realize a wide-variety of data-dependent acquisition strategies.

C. Predictor Performance

The system functionality was evaluated extensively using ECG signals from the MIT-BIH Arrhythmia database [12]. As an example, the predictor performance is illustrated in Fig. 6 over a dataset with slight heart-rate variability. The filter's ability to accurately track the quasi-periodic ECG with its typical slow variability and quickly adapt (after suffering from a missed prediction due to an abrupt variability, such as an arrhythmia) are clear. It should be noted that although the predictor cannot track extreme irregular cardiac activity (i.e., when the quasi-periodicity property doesn't hold), no compromise with the system's anomaly detection performance is made. This is because the case of persistent prediction errors is itself an anomaly indicator which can be used to take appropriate counter measures or stop the adaptive acquisition and capture these events with high accuracy. In other words, the predictor has a secondary functionality of acting as a simple, yet efficient, real-time anomaly detector while assisting AFE power savings over prolonged durations of slow HRV.

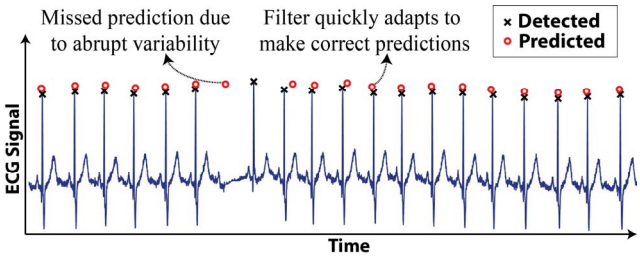

Fig. 6. Predictor performance in the presence of HRV.

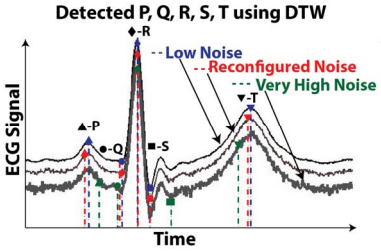

Peak Detection Errors

	$\sigma_{\Delta t}$ (ms)	$\sigma_{\Delta t}/T_{avg}$ (%)
Q	2.27	0.29
R	2.19	0.28
S	2.42	0.31
P	12.01	1.53
T	16.72	2.13

Fig. 7. DTW feature extraction performance.

D. Feature Extraction Performance

Since the feature extraction algorithms operate on transient waveforms to detect features that occur over only a small fraction of the period, selectively acquiring pristine data over limited regions of the cycle is sufficient for signal analysis while maintaining the same high detection accuracy for the features of interest. The results in Fig. 7 illustrate this benefit on ECG data from the Arrhythmia database played at the AFE's input. The detection accuracy is quantified in terms of the relative error $\sigma_{\Delta t}/T_{\text{avg}}$ where Δt is the difference in detected peak-position with data acquired adaptively relative to that acquired in high accuracy mode and T_{avg} is the average separation between consecutive detected peaks over the entire data. It can be observed from Fig. 7 that with data acquired adaptively, detection errors are 5× lower for Q-R-S peaks than those for P and T peaks (which are corrupted with greater noise) highlighting the selective detection accuracy. These results demonstrate that no compromise is made with the detection accuracy of the desired Q-R-S peaks of interest while slightly sacrificing the detection accuracy outside the desired Q-R-S region to save power. Additionally, it was found that high-noise levels as in [13] added behaviorally to the same known ECG result in inaccurate detections (>5% errors), thereby justifying the targeted noise-levels here. The predictive adaptation which depends upon these accurately detected R-peaks also thus remains unaffected with the dynamic reconfiguration.

TABLE I
PERFORMANCE SUMMARY AND COMPARISON TO EXISTING BIO-AFES

	This work	[13]	[1]	[2]	[14]	[3]
Application	ECG	ECG	ECG	ECG	ECG	ECG
Technology	65 nm	65 nm	180 nm	65 nm	180 nm	180 nm
Supply (V)	0.8	0.6	1.3	0.6	0.6	1.8
Amplifier						
Power (nW)	272 – 734#	1	559*	16.8	831*	10,600*
Gain (dB)	22 – 43	32	31-43	51 – 96	35 – 70	40 – 60
BW (Hz)	250	370	130	250	156	170
Integ. Noise (μV_{rms})	1.90 – 2.91#	26	4.9	6.52	3.44	1.1
CMRR (dB)	82	60	90	80	70	105
ADC						
Power (nW) @1 kSps	34.6**	1.1	67*	1.8 (.5 kSps)	19‡	4,400 (2 kSps)
Resolution	5-9	10	7-9	8	9	11
F_{sample} (kSps)	1-10	1.1-100	0.512	0.5	–	2
$ENOB_{max}$	8.75	9.2	8.96	7.14	8.01‡	10.6
INL (LSBs)	0.58	0.87	–	1.8	0.55	0.3
DNL (LSBs)	0.80	0.96	–	1	0.48	0.5
AFE System						
Power (nW)	307 – 769+	3	626	18.6	850	14,000
Tunable Knobs	Noise, Av, #Bits	–	Av, #Bits	Av	Av	Av, BW
P_{Amp}/P_{ADC}	7.86 – 21.2	0.91	8.34	9.33	43.74	2.41

+The DSP control and SAR logic were implemented off-chip on an FPGA and are not reported. **ADC in 9-bit mode.
#AFE in 35 dB gain mode. ‡Estimated from reported SNDR and FOM. *From reported component-wise breakdown.

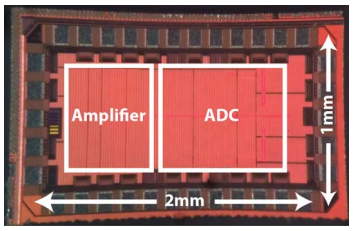

Fig. 8. Chip micrograph.

VI. CONCLUSION

In this paper, an ECG acquisition system with data-dependent power savings in the AFE using an LMS-aided noise-power reconfiguration was presented. As demonstrated, the proposed technique makes no compromise with the detection accuracy within the regions of interest or the anomaly detection capability of the system while achieving data-dependent 2.5× power reduction. Finally, Fig. 8 shows the chip micrograph and Table I provides a summary of the reconfigurable AFE. The table also indicates $P_{\text{Amp}}/P_{\text{ADC}}$ for such existing works to justify the focus on the amplifier power reduction in this work.

REFERENCES

[1] L. Yan *et al.*, "A 680nA fully integrated implantable ECG-acquisition IC with analog feature extraction," in *Proc. IEEE ISSCC Tech. Digest*, 2014, pp. 418–419.

[2] D. Jeon *et al.*, "An implantable 64nW ECG-monitoring mixed-signal SoC for arrhythmia diagnosis," in *Proc. IEEE ISSCC Tech. Digest*, 2014, pp. 416–417.

[3] R. F. Yazicioglu et al., "A 30 µW Analog Signal Processor ASIC for Portable Biopotential Signal Monitoring," *IEEE J. Solid-State Circuits*, vol. 46, no. 1, pp. 209–223, Jan. 2011.

[4] T. Yang et al., "A configurable 5.9 µW analog front-end for biosignal acquisition," in *Proc. IEEE CICC*, 2015, pp. 1–4.

[5] F. M. Yaul et al., "A 10b 0.6nW SAR ADC with data-dependent energy savings using LSB-first successive approximation," in *Proc. IEEE ISSCC Tech. Digest,* 2014, pp. 198–199.

[6] S. Jeong *et al.*, "A 120nW 8b Sub-ranging SAR ADC with Signal-Dependent Charge Recycling for Biomedical Applications," in *Proc. Symp. VLSI Circuits (VLSIC)*, pp. C60–C61, Jun. 2015.

[7] Q. Fan et al., "A 1.8 µW 60 nV/√Hz Capacitively-Coupled Chopper Instrumentation Amplifier in 65 nm CMOS for Wireless Sensor Nodes," *IEEE J. Solid-State Circuits*, vol. 46, no. 7, pp. 1534–1543, Jul. 2011.

[8] T. Denison et al., "A 2 µW 100 nV/√Hz Chopper-Stabilized Instrumentation Amplifier for Chronic Measurement of Neural Field Potentials," in *IEEE J. Solid-State Circuits*, vol. 42, no. 12, pp. 2934-2945, Dec. 2007.

[9] C. Li et al., "Detection of ECG characteristic points using wavelet transforms," *IEEE Trans. Biomed. Eng.*, vol. 42, no. 1, pp. 21–28, Jan. 1995.

[10] H. J. L. M. Vullings et al. , "Automated ECG segmentation with dynamic time warping," in *Proc. IEEE EMBC,* 1998, pp. 163–166 vol.1.

[11] C. Zong et al. , "Digitally Assisted Analog Front-end Power Management Strategy via Dynamic Reconfigurability for Robust Heart Rate Monitoring," *SIGBED Rev*, vol. 12, no. 3, pp. 36–39, Aug. 2015.

[12] MIT-BIH arrhythmia database - [Online]. Available: http://ww.physionet.org/physiobank/database/mitbh

[13] P. Harpe et al., "A 3nW signal-acquisition IC integrating an amplifier with 2.1 NEF and a 1.5fJ/conv-step ADC," in *Proc. IEEE ISSCC Tech. Digest*, 2015, pp. 1–3.

[14] M. Yip, J. L. Bohorquez, and A. P. Chandrakasan, "A 0.6V 2.9 W mixed-signal front-end for ECG monitoring," in *Proc. Symp. VLSI Circuits (VLSIC)*, 2012, pp. 66-67.